Results in Physics 39 (2022) 105768

Contents lists available at ScienceDirect

Results in Physics

journal homepage: www.elsevier.com/locate/rinp

Bloch points stabilization by means of diameter modulations in cylindrical nanowires

Guidobeth Sáez [a,1], Pablo Díaz [a], Nicolás Vidal-Silva [a,*], Juan Escrig [b,c], Eugenio E. Vogel [a,c]

[a] Departamento de Ciencias Físicas, Universidad de La Frontera, Casilla 54-D, 4811186 Temuco, Chile
[b] Departamento de Física, Universidad de Santiago de Chile (USACH), Avda. Víctor Jara 3493, Santiago, Chile
[c] Center for the Development of the Nanoscience and Nanotechnology (CEDENNA), Avda. Libertador Bernardo O'Higgins 3363, Santiago, Chile

ARTICLE INFO

Keywords:
Magnetic nanowires
Domain walls
Bloch points

ABSTRACT

The storage of information in long nanowires with a succession of independently oriented magnetic segments is of great practical use. It requires both the possibility of independently orienting the magnetization of each segment and great stability of the inscribed magnetization regarding spontaneous reversals. A practical way to separate sectors along the wire is by short modulations wider than the original wire that acts as a valve separating segments with independent magnetic orientations. When these two orientations are different, a Bloch Point (BP) develops within the modulation. It is precisely this BP that controls the stability of the system. In the present paper, we study the robustness of such BPs depending on geometrical parameters, such as the diameter and thickness of the cylindrical modulations as well as on external magnetic fields applied along the axis.

Introduction

Topological three-dimensional magnetic textures are currently an intriguing issue in spintronic and nanomagnetism due to the extraordinary properties that such structures possess and which have been proposed as a key ingredient for improving potential data storage, transport information, and microwave devices [1–5]. Within this class of magnetic structures, the most celebrated ones in the past decade are the skyrmions tubes [6,7], magnetic bobbers [8,9], magnetic hopfions [10,11], and Bloch Points (BP) singularities [12–15], the latter being the main subject of the present study. Notoriously, and because of their solitonic nature, all the aforementioned magnetic textures can be considered particle-like magnetic structures and present exotic topological properties when subjected to external means. In this sense, one of the main aspects to be considered regarding such topological properties is the emergent electrodynamics that appear when moving topological textures [16,17], as showed by the Skyrmion Hall effect in 2D magnetic media [18,19]. In terms of their stability, these exotic magnetic textures present topological protection under disturbances or lattice defects, which makes of them very attractive candidates as potential spintronic devices.

From a fundamental point of view, a BP can be defined as a magnetic singularity that usually leads to the transition between distinct magnetic configurations. Therefore, the BPs are identified as topological 3D magnetic solitons with a vanishing magnetization field at their center, which possesses remarkable topological properties. Specifically, in a closed surface around its center, the direction of the magnetization field covers the whole solid angle an integer number of times, i.e., if the norm of the magnetization field is preserved, it translates into a fundamental topological protection, which then gives the topological features. Thus, a BP is expected to be robust under perturbations and to give rise to an emergent electrodynamic [16], which might be evidenced by Hall-effect measurements [20].

A few examples of the importance of the presence of BPs in different systems are given next. In distinct magnetization processes, it has been shown that the annihilation of skyrmions confined to nanodots is mediated by the occurrence of BPs when such a process considers the contraction of the skyrmion's core [21,22]. Also, switching in the vortex core polarization is usually accompanied by the propagation of a BP [23]. Therefore, the presence, stability, and dynamics of controlled BP singularities are topics we must deal with when considering potential applications. For instance, the stabilization of a BP has been theoretically proposed by employing the self-magnetostatic field generated by a nanocube [24]. Similarly, micromagnetic simulations showed that a nanodisk with two layers of different chirality could host a stable and manipulable BPs [25]. Additionally, the center of a vortex domain

* Corresponding author.
E-mail address: nicolas.vidal@ufrontera.cl (N. Vidal-Silva).
[1] Present address: Departamento de Física, FCFM, Universidad de Chile, Santiago, Chile.

https://doi.org/10.1016/j.rinp.2022.105768
Received 26 April 2022; Received in revised form 10 June 2022; Accepted 26 June 2022
Available online 27 June 2022

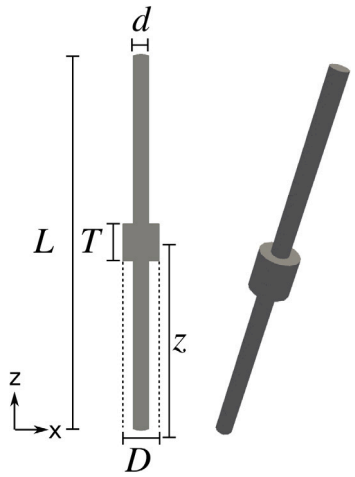

Fig. 1. Geometrical parameters define the system. L: length of the device; d: diameter of the cylindrical nanowire; D: diameter of the modulation concentric with the nanowire; T thickness of the modulation; z: modulation position along the symmetry axis.

wall configures itself a BP [26], so that the current knowledge about the stabilization of domain walls might bring us new insights on how to stabilize BPs.

Following that direction, a recent article showed that it is possible to store information in a succession of segments with different magnetic orientations [27]. When the concurring segments have a different orientation, the interface takes the form of a BP [28]. The reliability of the stored information depends on the stability of the BPs inside the modulations, and how to stabilize them becomes a challenging and motivating topic. Some previous reports contain interesting summaries of the variety of phenomena that appear at the domain walls along rod-like nanoparticles [26,29–34], including the presence of BPs, but none of them pay special attention to the conditions to control and stabilize them.

Here, we explore the possibility of stabilizing a BP in a diameter-modulated nanowire by modifying the geometry of the nanostructure. To test the stability, we apply external magnetic fields until the BP is ejected from the modulation. The main aim of the present work is then to find the conditions that allow to pin and stabilize the inscription of a BP inside a cylindrical modulation along a coaxial magnetic nanowire. This study covers spontaneous reversals as well as induced reversals triggered by externally applied magnetic fields. In this way, depinning fields for representative geometrical parameters will be reported.

Because of practical considerations, we cannot cover much of the configuration space, so that we will restrict ourselves to modulations of diameters D up to nearly twice the diameter d of the long central wire. The thickness T will be kept short enough (no larger than twice the diameter D) to avoid the shape anisotropy [35] favors magnetization orientation along the axis instead of the spacer (modulation) with a large perpendicular magnetization that is needed to separate segments as independent elements.

System and methodology

System

The system under consideration is a homogeneous cylindrical magnetic nanowire of diameter d and length L as shown to the left in Fig. 1. A coaxial cylindrical modulation is grown between the ends of the wire as part of the same single piece of material; such modulation is characterized by its diameter D ($D > d$) and thickness T. The position of the center of the modulation along the symmetry axis of the system is z; for the present paper $z = L/2$ since we are not interested in the influence of the ends of the wire. The diagram to the right in Fig. 1 gives a three-dimensional realization of the system.

We assume the magnetic material is nearly isotropic (like permalloy) and that the three sectors of the system can be independently magnetized. The segments to the end are long enough to ensure shape anisotropy, allowing permanent axial magnetization in any of the two directions. The thickness of the modulation is of the order of its diameter D, not becoming too long as to develop axial anisotropy of its own.

The length chosen for all the simulations is the same used in previous publications [27,36] to allow for comparisons: $L = 1100$ nm and $d = 50$ nm. Parameters D and T will be varied, as discussed below.

Initial conditions

To perform the simulations, we prepared the following initial conditions [36]. We assume that a counterclockwise vortex (looking from above) is initially inscribed in the external part of the modulation (excluding the core). The relative orientation of the magnetization of the segments defines four different cases: tail-to-head (TH), head-to-tail (HT), head-to-head (HH), and tail-to-tail (TT), naming the orientation of the lower segment first. Both TH and HT present no interface, so they end up aligning the modulation to have just one ferromagnetic domain. So, we are left with the last two cases as candidates for hosting a Bloch Point (BP).

Fig. 2 shows a HH orientation. To the left, we present the initially inscribed configuration: upwards magnetization in the segment below and downwards magnetization in the segment above; an abrupt Bloch domain wall (BW) is defined as presented within the continuous circle to the right; the discontinuous circle illustrates the initial magnetization of the middle plane of the modulation as seen from the top. On the right is the configuration spontaneously generated after a 5 ns simulation following the dynamics described in the next section; It can be observed that the BW developed into a BP and that the core is lost in the middle plane of the modulation, where a BP is clearly appreciated (details to be discussed in Section “Spontaneous configurations”).

Although our work intends to give a theoretical description of how the BP stabilization depends on the geometrical parameters of the selected system, one possible experimental way to inscribe a polarization as the one defined in Fig. 2 is to make use of the shape anisotropy presented by rods and disks due to their distinct aspect ratios [30,37]. Specifically, long wires will naturally develop axial anisotropy by means of the application of external magnetic fields. On the other hand, disks (such as the proposed modulation) tend to develop transverse or vortex domains in the planes perpendicular to the cylindrical axis. Therefore, by locating the system near the appropriate external magnetic fields is enough to ensure that the magnetic configuration in the modulation naturally converges to the one that their geometrical components allow. To achieve the head-to-head configuration proposed in Fig. 2 the segments can be located between the north poles of strong magnets or electromagnets. At the same time, on the central plane of the modulation and surrounding it, several curved magnets (like the usual horseshoe magnets) can be located to produce curling magnetization fields with the desired chirality to induce the vortex within the modulation. The resulting configuration will naturally minimize energy to reach a metastable state as presented in Fig. 2. Importantly, we have checked that even in the case that the initial condition would have a central core pointing along +−z, the resulting final state holds being a BP configuration. Nevertheless, other initial conditions (not considered here) might give rise to other metastable states, which is beyond the scope of the present study.

Simulation software and material parameters

To study and understand the stability of the confined BPs inside on modulation and the depinning processes, we have made use of Mumax3 [38] to solve numerically the Landau–Lifshitz–Gilbert equation given by

$$\frac{d\mathbf{m}}{dt} = -\frac{\gamma_0}{1+\alpha^2}\left[\mathbf{m}\times\mathbf{H}_{eff} + \alpha\mathbf{m}\times(\mathbf{m}\times\mathbf{H}_{eff})\right] \quad (1)$$

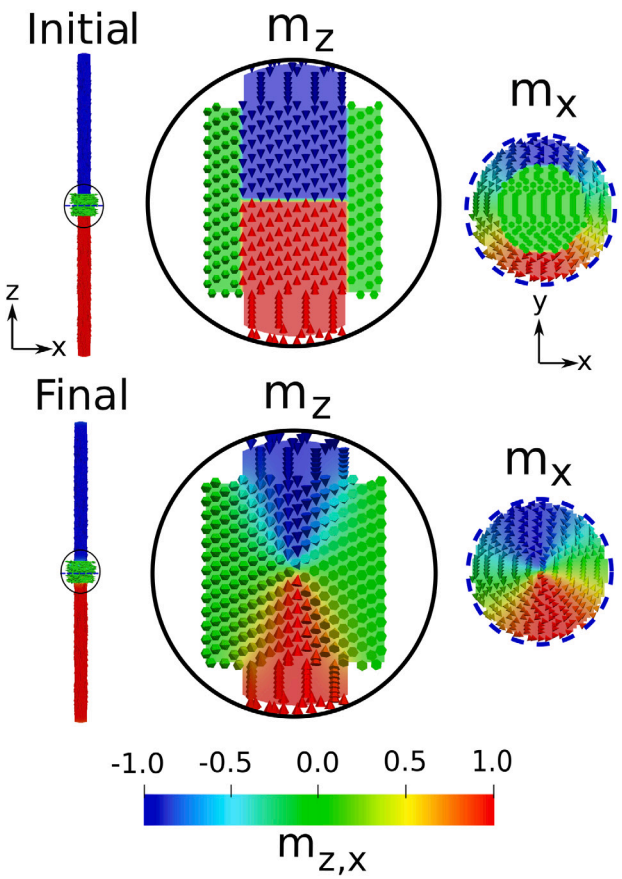

Fig. 2. (**Upper**) Illustration of the configuration initially inscribed. Here, we present a head-to-head (HH) configuration: the lower segment points its magnetization upwards (red), while the upper segment points its magnetization downwards (blue). A flat cross-section separates both segments, showing a Bloch Wall as the initial separation. A counter-clock vortex is inscribed at the modulation itself (except the core), looking from the top end. (**Lower**) This diagram presents the equilibrium magnetization after 5 ns of simulation. Full circles at the center highlight a vertical cut through the axis, showing how the Bloch Wall ends up in a Bloch Point. Dashed circles to the right isolate the cross-section through the middle of the modulation, showing how the vortex also absorbs the initial core of the modulation. The bar on the bottom indicates a color code for the magnetization component along the x- and z-axis. (For interpretation of the references to color in this figure legend, the reader is referred to the web version of this article.)

where $\mathbf{m}(r,t)$ is the normalized magnetization vector $\mathbf{m}(r,t) = \mathbf{M}(r,t)/M_s$, with M_s as the saturation magnetization, γ_0 is the gyromagnetic ratio and α is the Gilbert damping constant. The equation describes both the precession and relaxation motion of the magnetization in an effective field $\mathbf{H_{eff}}$. This effective field originates from the system interactions and it is obtained through the functional derivative $\mathbf{H_{eff}} = -\frac{1}{\mu_0 M_s}\frac{\delta\varepsilon[\mathbf{m}]}{\delta\mathbf{m}}$ of the energy density functional (see Eq. (2)), where μ_0 is a magnetic constant. This functional is originated by the internal interactions E_{int} of the system given by the exchange energy E_{exc} and dipolar E_{dip} and the external ones as the Zeeman energy E_{Zeeman}.

$$E[\mathbf{m}] = E_{exc} + E_{dip} + E_{Zeeman} = \int_V \varepsilon[\mathbf{m}]\, dV$$
$$= \int_V \left(A\sum_{i=1}^{3}(\nabla m_i)^2 - \frac{\mu_0}{2}\mathbf{H_{dip}}\cdot\mathbf{M} - \mu_0\mathbf{H}_{ext}\cdot\mathbf{M}\right) dV \qquad (2)$$

We consider permalloy as the material used in the simulations, with its properties summarized by the following parameters [39]: saturation magnetization $M_s = 800\times10^3$ A/m; stiffness constant $A = 13\times10^{-12}$ J/m. We have used cell sizes of $2\times2\times2$ nm^3 and the damping constant is chosen to a fix value of $\alpha = 0.1$, to appreciate the dynamics of magnetization and solve the LLG equation during 5 ns. This time was tested to be sufficient for the system to reach equilibrium after the depinning process.

Results and discussions

Spontaneous configurations

Fig. 2 picks a representative configuration to illustrate the way simulations are done. An entirely equivalent situation develops for a TT orientation, so we will stick to HH configurations from now on. This procedure is repeated through the parameter space. Fig. 3(a) presents the final configurations for D increasing from left to right in the interval [60,110] nm at a pace of 10 nm; T increases from top to bottom in the range [60,110] with increments of 10 nm; while Fig. 3(b) corresponds to a closed-up view of the extreme cases in our parameters space, i.e., $T = D = 60$ nm and $T = D = 110$ nm. The bar to the right gives the color code for the magnetization orientations. A double cone with opposite magnetization orientations develops inside the modulation immerse in the disk, initially dominated by a vortex. The flat BW has developed into a small region with zero or nearly zero magnetization, which is the main characteristic of a BP.

Despite the similarity of the configurations in Fig. 3, subtle differences in the magnetization orientations are to be noticed. The red color (FM upwards) is separated from the green color (vortex) by a yellow cone (mixed magnetization). Similarly, the blue color (FM downwards) is separated from the green color (vortex) by a cyan cone (mixed magnetization). These yellow and cyan cones are wider for longer and thinner modulations, which points to instability for the configuration; eventually, an external agent could erase the stored magnetization. Yellow and cyan cones are almost absent for shorter and thicker modulations, evidencing a clean cut between magnetic phases and a better definition of the BP. With longer and thinner modulations, the vortex mass is partially lost to the benefit of one of the FM domains. The BP is displaced from the center, trying to escape through one end of the modulation.

Several comments are in order. First, all these configurations hold a BP, which keeps the property of TT (or HH) orientations. Second, the sharpest definition of a BP is reached for wide and short modulations (D = 110 nm, T = 60 nm, in Fig. 3). Third, long and narrow modulations (D = 60 nm, T = 110 nm, in Fig. 3) give a BP migrated from the center position evidencing fluctuations tending to destabilize the BP. Fourth, although wider modulations better stabilize the BP, they could be challenging to achieve experimentally; for this reason, we will look for intermediate D values. Fifth, configurations with D = 70–80 nm and T = 70–80 nm look realizable. We settle for a configuration with D = 80 nm and T = 80 nm as a prototype of a device based on diameter modulated magnetic nanowires.

Magnetic fields

An external magnetic field along the symmetry axis was applied to the spontaneously stabilized configurations. The procedure is: the systems always start in the original state shown in Fig. 3. Then a homogeneous magnetic field of intensity H_z is instantly applied to the system, and the simulation goes for 5 ns. The magnetization $M_Z(t)$ is recorded every 0.01 ns. In the end, the magnetic field is suppressed. Then, a new simulation begins with the same original state, the external field is set to a new value $H_z + \Delta H$, and a new simulation of 5 ns is run. It goes like this until all the desired fields have been invoked. In Fig. 4 only 1 ns is represented, but no changes were noticed beyond this range up to 5 ns.

Fig. 4 illustrates the z component of the total magnetization $M_Z(t)$ of the device with respect to the saturation magnetization (when the system is one ferromagnetic monodomain). Geometrical parameters correspond to a modulation with T = 80 and D = 80 nm. The response

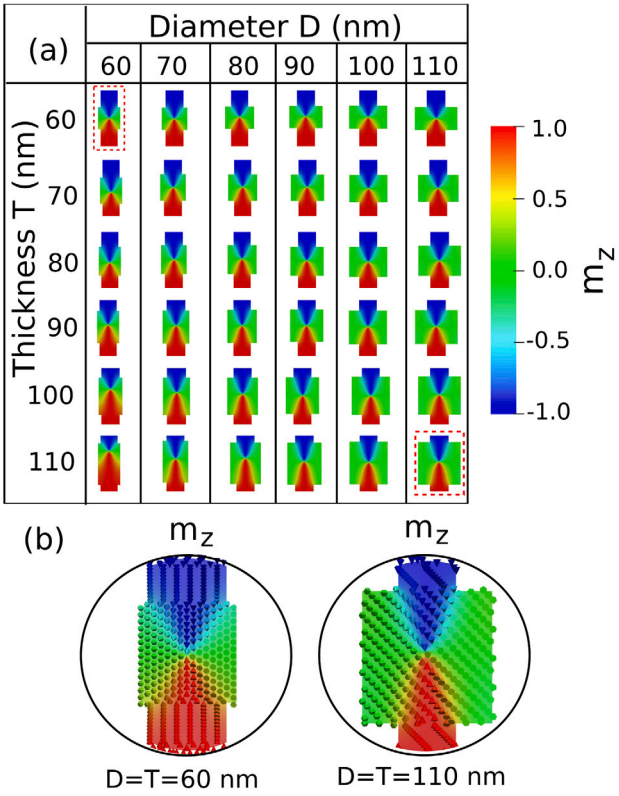

Fig. 3. (a) Phase diagram giving the final configurations for the most relevant systems considered in this study. Magnetization orientation is given by the color codes to the right. (b) A closed up view of the cases $D = T = 60$ nm (left) and $D = T = 110$ nm (right) showing the difference between the internal magnetic configuration for each geometry. (For interpretation of the references to color in this figure legend, the reader is referred to the web version of this article.)

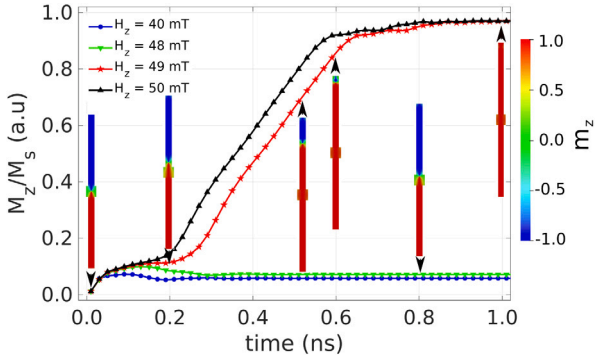

Fig. 4. Evolution of the normalized magnetization (M_Z/M_S) of the system for 4 different external magnetic fields as given in the inset. At least a field of 49 mT is needed to reverse the magnetization: this is the depinning field of the device with $D = 80$ nm and $T = 80$ nm. Arrows link the snapshot to the point on the corresponding curve.

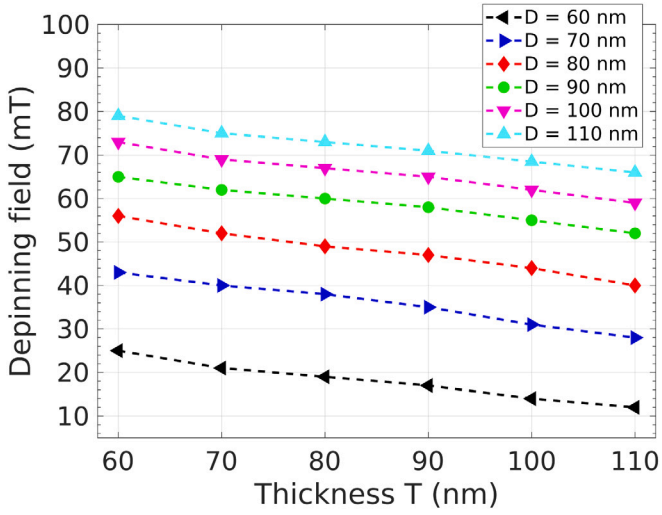

Fig. 5. Depinning field for the configurations presented if Fig. 3. Diameter of the modulations are given in the inset along with the symbols identifying actual measurements. Dashed lines are only a guide for the eyes.

of the system to four different intensities of the external field H_Z are shown: 40 mT, 48 mT, 49 mT, and 50 mT. A marginal increase in the magnetization is appreciated when going from 40 mT to 48 mT probably due to alignments at the ends and borders. However, a completely different behavior is noticed for a field of 49 mT: there are no differences with previous curves for the first 0.20 ns, but from there on to about 0.65 ns an almost linear increase of $M_Z(t)$ is got; then the magnetization flattens with small increases because of marginal alignments. Under a field of 50 mT, the situation is like the previous one only shifted to shorter times. In this way, we identify the depinning field of this system as the first field for which the normalized magnetization tends to 1.0 after a time of a couple of ns. For the present example, such a depinning field is 49 mT.

Snapshots in Fig. 4 are illustrative of the dynamics of the system under external magnetic fields. The first one to the left represents the original condition coincident with the configuration for $D = 80$ nm and $T = 80$ nm in Fig. 3. It is followed by one obtained at $t = 0.2$ ns, corresponding to the curve for 49 mT, when the BP is just on the verge of abandoning the modulation, leaving it as an upward ferromagnetic domain. The third snapshot represents the field condition when the BP is transiting to the upper end. The condition in which the BP vanishes is presented by the fourth snapshot. Relative to the other curves, the last snapshot to the right presents the saturated and stable condition of a ferromagnetic monodomain reached even before 1 ns. Previously, the fifth snapshot applies to the lower curves illustrating the low and stable magnetization reached for fields under 49 mT; the BP appears slightly displaced from the center of the modulation, but not enough to abandon it.

Fig. 5 presents the thickness dependence of the depinning field for modulations of different thickness as presented in the inset. The general tendency indicates the depinning field slightly decreases for longer modulations. This agrees with the general trend of ferromagnetic domains for longer elements. Shorter modulations are harder to align their magnetization along the axis. A vertical look across the different diameters tells that wider modulations require larger depinning fields. However, the increase in the depinning field is faster for shorter diameters as compared with the modest gain, as D gets over 100 nm. Wide modulations could be difficult to achieve experimentally. In summary, modulations with geometrical parameters at the center of this diagram require depinning fields of the order of 50 mT, which is safe enough for most of the random magnetic fields a storage device can find in daily life [40].

Conclusions

A single coaxial modulation grown at the center of a long magnetic nanowire is enough to host a BP inside. In a HH (or TT) configuration, a metastable state is reached with the modulation presenting a vortex with any chirality and the two segments host opposite magnetization orientations.

A phase diagram shows that despite a general convergence to metastable states with the BP near the center of the modulation, weakening signs appear for long and narrow modulations. On the other

extreme, short and wide modulations offer very stable conditions for retaining the BP even for external fields of about 80 mT.

However, wide modulations are difficult to obtain, so we continued the analysis for an intermediate case to test the dynamics of the device in the presence of external axial magnetic fields.

For the case of an eventual device with $D = 80$ nm and $T = 80$ nm, a field of 49 mT along the z axis is needed to expel the BP from the modulation which unfolds a steady motion of the BP along the segment to the end of the wire to disappear finally.

Results here were obtained for a likely configuration, but characteristics can be altered to describe different systems intended to store magnetic fields within successive independent sectors along a magnetic nanowire. Simple modulations of the same materials could be enough to serve as safe separators of ferromagnetic domains with diverse magnetic orientations along the device.

CRediT authorship contribution statement

Guidobeth Sáez: Conceptualization, Software, Visualization, Formal analysis. **Pablo Díaz:** Conceptualization, Methodology, Formal analysis, Writing – original draft. **Nicolás Vidal-Silva:** Conceptualization, Methodology, Formal analysis, Writing – original draft. **Juan Escrig:** Conceptualization, Resources, Formal analysis, Writing – original draft. **Eugenio E. Vogel:** Conceptualization, Resources, Formal analysis, Writing – original draft.

Declaration of competing interest

The authors declare that they have no known competing financial interests or personal relationships that could have appeared to influence the work reported in this paper.

Data availability

Data will be made available on request.

Acknowledgments

E.V., P.D. and J.E. acknowledge support from the following Chilean sources: Fondecyt (Chile) under contracts 1190036 and 1200302 respectively, and Financiamiento Basal para Centros Científicos *y* Tecnológicos de Excelencia (Chile) through the Center for Nanoscience and Nanotechnology (CEDENNA, ANID Contract AFB180001). N.V.-S. acknowledges Fondecyt Iniciación, Chile Grant No. 11220046 and G.S acknowledges ANID- Subdirección de Capital Humano/Doctorado, Chile Nacional/2022- 21222167.

References

[1] Fernández-Pacheco A, Streubel R, Fruchart O, Hertel R, Fischer P, Cowburn RP. Nature Commun 2017;8(1):1–14.
[2] Fischer P, Sanz-Hernández D, Streubel R, Fernández-Pacheco A. APL Mater 2020;8(1):010701.
[3] Staño M, Fruchart O. Handbook of magnetic materials, Vol. 27. Elsevier; 2018, p. 155–267.
[4] Elías R, Carvalho-Santos V, Núñez A, Verga A. Phys Rev B 2014;90(22):224414.
[5] Göbel B, Mertig I, Tretiakov OA. Phys Rep 2021;895:1–28.
[6] Wolf D, Schneider S, Röß ler UK, Kovács A, Schmidt M, Dunin-Borkowski RE, Büchner B, Rellinghaus B, Lubk A. Nature Nanotechnol 2021;1–6.
[7] Birch M, Cortés-Ortuño D, Turnbull L, Wilson M, Groß F, Träger N, Laurenson A, Bukin N, Moody S, Weigand M, et al. Nature Commun 2020;11(1):1–8.
[8] Zheng F, Rybakov FN, Borisov AB, Song D, Wang S, Li Z-A, Du H, Kiselev NS, Caron J, Kovács A, et al. Nature Nanotechnol 2018;13(6):451–5.
[9] Ahmed AS, Rowland J, Esser BD, Dunsiger SR, McComb DW, Randeria M, Kawakami RK. Phys Rev Mater 2018;2(4):041401.
[10] Liu Y, Hou W, Han X, Zang J. Phys Rev Lett 2020;124(12):127204.
[11] Sutcliffe P. J Phys A 2018;51(37):375401.
[12] Feldtkeller E. Z Angew Phys 1965;19(6):530–+.
[13] Döring W. J Appl Phys 1968;39(2):1006–7.
[14] Pylypovskyi OV, Sheka DD, Gaididei Y. Phys Rev B 2012;85(22):224401.
[15] Elías RG, Verga A. Eur Phys J B 2011;82(2):159–66.
[16] Schulz T, Ritz R, Bauer A, Halder M, Wagner M, Franz C, Pfleiderer C, Everschor K, Garst M, Rosch A. Nat Phys 2012;8(4):301–4.
[17] Göbel B, Mook A, Henk J, Mertig I, Tretiakov OA. Phys Rev B 2019;99(6):060407.
[18] Chen G. Nat Phys 2017;13(2):112–3.
[19] Jiang W, Zhang X, Yu G, Zhang W, Wang X, Benjamin Jungfleisch M, Pearson JE, Cheng X, Heinonen O, Wang KL, et al. Nat Phys 2017;13(2):162–9.
[20] Tejo F, Heredero RH, Chubykalo-Fesenko O, Guslienko K. Sci Rep 2021;11(1):1–9.
[21] Birch MT, Cortés-Ortuño D, Khanh ND, Seki S, Štefančič A, Balakrishnan G, Tokura Y, Hatton PD. Commun Phys 2021;4(1):1–9.
[22] Li Y, Mankovsky S, Polesya S, Ebert H, Moutafis C, et al. Phys Rev B 2021;104(14):L140409.
[23] Thiaville A, García JM, Miltat J, Schrefl T, et al. Phys Rev B 2003;67(9):094410.
[24] Charilaou M. Phys Rev B 2020;102(1):014430.
[25] Beg M, Pepper RA, Cortés-Ortuño D, Atie B, Bisotti M-A, Downing G, Kluyver T, Hovorka O, Fangohr H. Sci Rep 2019;9(1):1–8.
[26] Hertel R, Kirschner J. Physica B 2004;343(1–4):206–10.
[27] Sáez G, Díaz P, Cisternas E, Vogel EE, Escrig J. Sci Rep 2021;11(1):1–9.
[28] Da Col S, Jamet S, Rougemaille N, Locatelli A, Mentes TO, Burgos BS, Afid R, Darques M, Cagnon L, Toussaint J-C, et al. Phys Rev B 2014;89(18):180405.
[29] Fernández-Roldán JA, Ivanov YP, Chubykalo-Fesenko O. Magnetic nano-and microwires. Elsevier; 2020, p. 403–26.
[30] Moreno R, Carvalho-Santos V, Altbir D, Chubykalo-Fesenko O. J Magn Magn Mater 2022;542:168495.
[31] Niedoba H, Labrune M. Eur Phys J B 2005;47(4):467–78.
[32] Ferguson C, MacLaren D, McVitie S. J Magn Magn Mater 2015;381:457–62.
[33] Hertel R. J Phys: Condens Matter 2016;28(48):483002.
[34] Ivanov YP, Vázquez M, Chubykalo-Fesenko O. J Phys D: Appl Phys 2013;46(48):485001.
[35] e Castro Jd, Altbir D, Retamal J, Vargas P. Phys Rev Lett 2002;88(23):237202.
[36] Sáez G, Saavedra E, Vidal-Silva N, Escrig J, Vogel EE. Results Phys 2022;37:105530.
[37] Landeros P, Escrig J, Altbir D, Laroze D, e Castro Jd, Vargas P. Phys Rev B 2005;71(9):094435.
[38] Vansteenkiste A, Leliaert J, Dvornik M, Helsen M, Garcia-Sanchez F, Van Waeyenberge B. AIP Adv 2014;4(10):107133.
[39] Sáez G, Cisternas E, Diaz P, Vogel EE, Burr JP, Saavedra E, Escrig J. J Magn Magn Mater 2020;512:167045.
[40] Kovac D, I. K. Adv Electr Electron Eng 2011;183–6, http://2q3-fsx.257.cz/index.php/AEEE/article/view/124/109.